A Microvision-Based Motion Measurement System for Nanopositioners Using the Feature-to-Phase Method

Sheng Yao, Xianmin Zhang, Benliang Zhu, Hai Li, Longhuan Yu, and Sergej Fatikow

***Abstract*— The development of automation at the nanoscale has been calling for precision motion sensing for robotic nanopositioners. This study presents a microvision-based measurement system for the accurate and efficient motion sensing of three-degree-of-freedom (DOF) nanopositioners. In this measurement system, an optimized target searching (OTS) scheme is proposed for automatic tracking target selection. A strategy is designed to combine feature matching with phase correlation to balance the measurement accuracy and efficiency. By proposing a multiple target tracking scheme, high-precision angular measurement is achieved, and velocity estimation is also provided in this microvision-based measurement system. Subsequently, offline simulations and online experiments are performed to comprehensively evaluate the performances of the microvision-based system with comparisons to traditional instrumentation. The simulation and experimental results demonstrate that the proposed system and marker-free method can realize excellent extensibility, strong robustness, and high precision of motion tracking for the nanopositioners, with measurement accuracy higher than 93 nm and 96 μrad.**

***Index Terms*— Feature matching, marker-free tracking, microvision-based sensing, motion measurement, nanopositioner, phase correlation, robotic micromanipulation, velocity estimation.**

I. Introduction

NANOPOSITIONER is a type of mechatronic system that aims to provide motion at small scales. It has been playing a key role in precision engineering, including micro/nano- manipulation [1], scanning probe microscopy [2], and biomedical characterization [3]. With the research community's efforts, high positioning resolution, precision motion control, and fast response have been achieved by the robotic nanopositioners [4]. Meanwhile, the advancement of nanopositioners puts forward the demand for precision motion sensing. Current commercial instruments for nanopositioners, such as laser interferometers, grating scales, and capacitive sensors (CSs), are only capable of high-accuracy measurement in a single degree of freedom (DOF), while multiple sensors and complex structures have to be employed for multi-DOF motion measurement. For instance, Torralba et al. [5] delicately designed a structure to install a laser interferometer system inside the nanopositioner for multi-DOF measurement. Li et al. [6] presented a six-DOF measurement system based on the scale grating technique with multiple beam splitters and mirrors. Wang and Zhang [7] manufactured a specific structure for six capacity sensors to measure the displacement of a planar three-DOF nanopositioner. Since these traditional instruments often required auxiliary devices, tricky installation, and customized structure, their practicality was inevitably limited.

Motion measurement by computer microvision is a noninvasive method with attractive properties, such as multi-DOF measurement ability, direct visualization, easy integration, and tremendous available sensing information [8]. The existing microvision-based motion measurement methods in precision engineering can be classified into three categories, namely, template-based method, feature-based method, and phase-based method. The template-based method directly matches the template according to the pixel intensity, which can be further divided into two subcategories by different searching strategies: the exhaustive approach and the iterative approach. For example, Zhao et al. [9] applied bilinear interpolation into the template-based method for displacement measurement of the nanopositioner with nanometer accuracy. However, the computational cost of the exhaustive approach was expensive, and high-speed tracking was not achieved. Li et al. [10] implemented two-DOF real-time motion measurement of the nanopositioner by the iterative approach. Nevertheless, the large motion measurement between two consecutive images was not available, since the iterative approach only searched the template in its neighborhood. The tracking performance of the template-based method is also significantly dependent on template selection, which often requires manual intervention.

For the feature-based method, motion measurement is achieved by tracking the features, which are extracted by the feature detectors from the image and then encoded into

Manuscript received 28 September 2022; accepted 8 December 2022. Date of publication 4 January 2023; date of current version 12 January 2023. This work was supported by the National Natural Science Foundation of China (NSFC) under Grant 51820105007 and Grant 51905176. The Associate Editor coordinating the review process was Dr. Jochen Lang. *(Corresponding authors: Sheng Yao; Xianmin Zhang.)*

Sheng Yao is with the School of Biomedical Engineering, the Guangdong Provincial Key Laboratory of Medical Image Processing, and the Guangdong Province Engineering Laboratory for Medical Imaging and Diagnostic Technology, Southern Medical University, Guangzhou 510515, China (e-mail: yaosheng@smu.edu.cn).

Xianmin Zhang, Benliang Zhu, Hai Li, and Longhuan Yu are with the Guangdong Key Laboratory of Precision Equipment and Manufacturing Technology, School of Mechanical and Automotive Engineering, South China University of Technology, Guangzhou 510640, China (e-mail: zhangxm@scut.edu.cn; meblzhu@scut.edu.cn; lihai@scut.edu.cn; hans_longhuan@163.com).

Sergej Fatikow is with the Division of Microrobotics and Control Engineering, Department of Computing Science, University of Oldenburg, 26129 Oldenburg, Germany (e-mail: sergej.fatikow@uni-oldenburg.de).

Digital Object Identifier 10.1109/TIM.2023.3234038

the local descriptors. Although the feature-based method is expected to be more efficient and less sensitive to environmental variations [11], normally only the integer-pixel matching accuracy is obtained due to the property of the sparse point correspondence. On the other hand, the phase-based method can achieve high accuracy by retrieving spatial displacement from the phase shift between acquired images [12]. However, processing the whole Fourier spectrum is computationally expensive. Many efforts focus on improving the efficiency of the phase-based method. For example, Andre et al. [13] designed an encoded periodic pattern for efficient motion tracking at the nanoscale. Yamahata et al. [14] utilized the periodic microstructure in microelectromechanical systems (MEMS) for high-accuracy displacement measurement. Nevertheless, artificial markers such as encoded or repeating patterns were required in these studies to evaluate fewer spectral components. Our earlier work [15] developed an optical microvision system for full-field displacement measurement. However, the computation of the previous method was too costly for real-time motion tracking. Therefore, we are motivated to develop a novel full field-of-view (FOV) micromotion tracking method without installing artificial targets, which combines the advantages of the high efficiency from the feature-based method and the high accuracy from the phase-based method.

In this study, a marker-free microvision-based measurement system is proposed that aims to track three-DOF micromotion of nanopositioners at a high frame rate. The effectiveness of the proposed microvision-based motion tracking method is verified by both offline simulation and online experimental studies. The remainder of this article is presented as fellows. The microvision-based measurement system and the mathematical problems of three-DOF motion measurement are stated in Section II. In Section III, a micromotion tracking method that considers both efficiency and accuracy is presented in detail. Section IV evaluates the proposed method with offline simulation, and online experiments are conducted in Section V. Finally, Section VI concludes this article.

II. Microvision-Based Motion Tracking: Problem Statement

A. Problem Statements and Objectives

To achieve flexible and high-precision motion tracking of the nanopositioners, a few issues need to be addressed.

1) There is always a trade-off between tracking precision and efficiency for the microvision-based methods. Maintaining a high accuracy during online measurement without dropping the processing frame rate is crucial.
2) To eliminate the need to manufacture and install artificial targets, tracking natural textures on the nanopositioners is preferred.
3) Since the tracking target quality often influences the performance, an automatic target selection approach needs to be designed.
4) High automation and easy accessibility of micromotion tracking are favored, so that the method can be available for users from different research backgrounds.

Real-time micromotion measurement can be realized by extracting and tracking the natural feature on the nanopositioners. Assume f_t is the feature detected in the current frame of the image sequence, f_0 is the feature position in the previous frame, the three-DOF micromotion $\boldsymbol{m} = (d_x, d_y, \theta)$ can be estimated by

$$\boldsymbol{m} = \operatorname{argmin} \sum_{\boldsymbol{x} \in I} F(f_t(\boldsymbol{x}; \boldsymbol{m}), f_0(\boldsymbol{x})) \tag{1}$$

where $\boldsymbol{x} = (\mu, \nu)$ is the feature location in the image coordinate I, F is the distance function between f_t and f_0, as shown in Fig. 1. Therefore, a proper approach is needed to strike a balance between the accuracy and efficiency of updating micromotion $\boldsymbol{m}$ in (1).

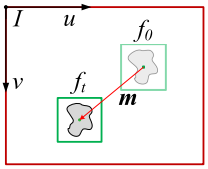

Fig. 1. Microvision-based motion estimation using the natural textures.

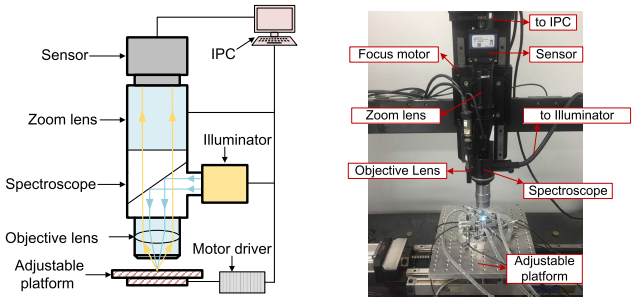

Fig. 2. Microvision-based measurement system architecture. (a) Schematic of the microvision optical design. (b) Detailed hardware configuration of the proposed microvision system.

B. System Architecture

An optical microvision-based measurement platform, which consists of an optical imaging unit, a loading unit, and an image processing unit, has been developed [15]. As shown in Fig. 2, the light is emitted from the illuminator, which is then led by the spectroscope through the objective lens. After illuminating the measured target, the sensor captures the reflected light through the zoom lens and then sends the image data to the image processing unit. Using such an optical imaging unit, the high-quality brightness of the images with a short exposure time for video-rate image acquisition can be achieved. To sense the micromotion of the nanopositioner, one can place the nanopositioner on the loading platform of the microvision system, which can carry the nanopositioner to the FOV. Then, the motorized focus can be adjusted to the surface of the nanopositioner, so that the micromotion can be captured by the image sensor and the frame grabber. By implementing the image processing algorithm in the industrial personal computer (IPC), micromotion tracking can be realized.

III. Methodology

A. Optimized Target Searching (OTS) Scheme

In most cases, an ideal tracking target normally contains salient textures, which is chosen manually. Manual target

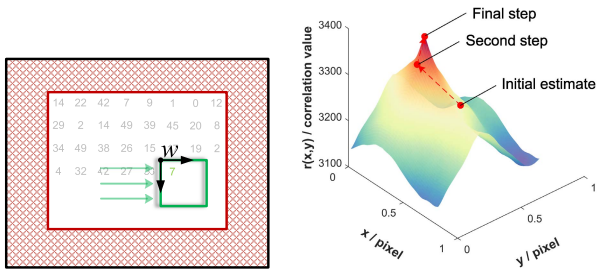

Fig. 3. Illustrations of (a) OTS scheme and (b) subpixel phase correlation, where the red dashed line illustrates the path for locating the correlation peak.

selection requires related training and stringent skills, but still may cause tracking performance deterioration due to the variations of manual selections by different human operators. A bad choice of the target may significantly deteriorate the tracking performance in efficiency and accuracy. To automate the target selection process, a quantitative indicator from the microvision image is required. As a result, an OTS scheme is proposed based on feature extraction.

Image feature refers to specific structures, such as keypoints and blobs, that can represent certain properties in a region. Consequently, features are extracted and utilized from the microvision image to evaluate the quality of tracking target selection. Feature extraction includes two steps, namely feature detection and description. Features from accelerated segment test (FAST) detector [16] is applied to process the excellent efficiency, where a circle c with the radius of 9 pixels around the candidate keypoint p is selected for keypoint detection.

A search window w is set to slide over the FOV of the microvision system, as illustrated in Fig. 3(a), where the feature detection is conducted within the window w. At each step, both the location and the number of detected keypoints are recorded. Using this exhaustive search approach, the region with the most number of keypoints can be selected as the tracking target, as more keypoints can enhance the tracking robustness. The additional procedures are also designed in the OTS scheme to ensure effective micromotion tracking: 1) the searching path is from the top left to the bottom right of the FOV, and the step size of the search window w is set as the same value as the circular radius of FAST detector; 2) if multiple regions score the same most number of keypoints, the central location will be chosen as the tracking target; and 3) if the target is moving out of the FOV, the tracked target will be lost. Thus the area near the FOV boundary is disabled from searching, in which the area size is set according to the motion range of the nanopositioner.

As presented in Pseudocode 1, the OTS scheme can automatically select the tracking target with the most features in the FOV of the microvision system, which is hard to quantify by human vision. Once the proper tracking target on the nanopositioner is selected, the initialization process is completed, and the microvision-based method is ready for stable motion measurement.

Pseudocode 1: Optimized Target Searching (OTS)

Input : Image sequence I_t.
Output: Tracking target T.
if $t == 0$ **then**
  Set the size of Fast detector and the step for the search window w;
  Set the area disable for tracking target searching;
  Extract keypoint p in the FOV with the search window w;
  Label the keypoint number at each location;
  Sort the candidate regions according to their keypoint number: $C_1 \geq C_2 \geq C_3 \geq \ldots \geq C_n$;
  if $C_1 = \ldots = C_i$ **then** `// multiple regions score the same most number of keypoints`
    Choose the region near to the center of FOV $C_k \subset (C_1, \ldots, C_i)$;
    $T \leftarrow R_k$;
  else
    $T \leftarrow R_1$;

B. Fast Feature-Based Method for Coarse Motion Estimation

After the tracking target T is confirmed by the OTS scheme, the keypoints within the target region are selected as the tracking feature. To obtain orientation information, the intensity centroid approach is employed. The intensity centroid of the feature neighborhood c can be calculated by the image moments M_{ij}, and the orientation is assigned to each keypoint as

$$\begin{cases} \theta = \arctan\dfrac{M_{01}}{M_{10}} \\ M_{ij} = \displaystyle\sum_x \sum_y x^i y^j I(x, y). \end{cases} \tag{2}$$

Then, the detected keypoints are constructed into the feature descriptor as a form of image representation. The float-point-based descriptors, such as scale invariant feature transform (SIFT) [11] and speeded-up robust features (SURF) [17], impose a relatively large computational burden on the high-efficiency motion measurement task. The binary-string-based feature descriptors, on the other hand, convert detected keypoints into binary feature vectors that only contain 0 and 1. They have high computational efficiency, which is more suitable for the real-time systems. As a result, rotated binary robust independent elementary feature (rBRIEF) suggested in [18] is applied in the feature description. Concretely, each keypoint in (2) is encoded into a vector of n binary tests

$$b(n) = \sum_{1<i<n} 2^{i-1} \tau(I; \mu_i, \nu_i) \tag{3}$$

where τ is equal to 1 or 0 depending on the pixel intensity, μ and ν represent the pair of pixels in the neighborhood of keypoints with the properties of high variance and low correlation, so that each feature description can obtain high distinguishability. The keypoint orientation θ is also attached to the descriptor $b^*(I, \theta) = f(n) \in R_\theta S$, where S is the keypoint neighborhood location matrix and R_θ is the corresponding rotation matrix.

After the target T is encoded into the feature descriptor, feature matching is conducted with a new input image from the

image sequence I_t. All keypoints from the new image are also constructed into the feature descriptor, and then evaluated with the descriptors from the tracking target by Hamming distance

$$H(T, I_t) = \sum_{i=1}^{p} b_i^*(T) \otimes b_i^*(I_t) \tag{4}$$

where l is the feature point number, $b_i^*(T) \in (0,1)^p$ and $b_i^*(I_t) \in (0,1)^p$ denote the binary-string-based descriptors extracted from the tracking target T and the input image I_t, respectively, $\otimes$ represents the bitwise XOR operation.

The approximate nearest neighbor search [19] is adopted for fast descriptor matching. Once the feature descriptors are matched, the quartiles approach [20] is used to discard outliers while estimating the geometric transformation. Then, the region in the input image that fits the feature with the tracking target is obtained, and the coarse motion $\boldsymbol{m}_c$ is recorded. The fast feature-based method not only provides full FOV coarse motion estimation with high effciency, but also shrinks the searching scope for fine motion estimation, therefore further raising the speed afterward.

C. Subpixel Phase Correlation for Fine Motion Estimation

According to the aforementioned procedure, the tracking target has been coarsely located in integer-pixel accuracy, followed by fine micromotion estimation using the phase-based method. A region of interest (ROI) R with the same size of tracking target T is obtained for subpixel micromotion measurement, which can avoid the high-computational cost from phase correlation of the full resolution images, meanwhile maintain its remarkable advantage: high matching accuracy.

Based on a linear relationship, namely the phase-to-displacement relationship, the target displacement results in the phase shift of the Fourier transform (FT), which can be expressed as

$$\mathcal{F}\big(I\big(\boldsymbol{x} - \boldsymbol{m}_f\big)\big) = \mathcal{F}(I(\boldsymbol{x})) \cdot e^{-2\pi i \boldsymbol{m}_f \xi} \tag{5}$$

where $\mathcal{F}$ denotes the FT, $\boldsymbol{x} = [x, y]$ is the spatial coordinate, $I(\boldsymbol{x})$ stands for the pixel intensity, ξ is the transform variable of $\boldsymbol{x}$, and $\boldsymbol{m}_f$ represents the spatial displacement, also the fine motion yet to be estimated. Let the target $T(\boldsymbol{x})$ be $f(\boldsymbol{x})$, the ROI $R(x)$ be $g(\boldsymbol{x})$, the phase correlation can be given as

$$r(\boldsymbol{x}) = \sum_{\boldsymbol{x}} f(\boldsymbol{x}) g^*\big(\boldsymbol{x} - \boldsymbol{m}_f\big) = F(\boldsymbol{x}) G^*(\boldsymbol{x}) e^{-2\pi i \boldsymbol{m}_f \xi} \tag{6}$$

where the summation is taken over the image pixels, $*$ represents complex conjugation, F and G denote the FT of f and g, respectively. The fine motion $\boldsymbol{m}_f$ can be reconstructed by phase retrieval, which is locating the peak coordinates of the phase correlation function

$$\boldsymbol{m}_f = \underset{x}{\operatorname{argmax}}\{r(\boldsymbol{x})\}. \tag{7}$$

To achieve subpixel measurement accuracy, the upsampling technique [21] is used. Concretely, assume the subpixel factor is λ $(0 < \lambda < 1)$, and both T and R size are $M \times N$, by embedding $F(\boldsymbol{x})G^*(\boldsymbol{x})$ into a larger zero array with the size $(M/\lambda) \times (N/\lambda)$, the upsampled correlation peak can be found after computing the inverse FT, and the subpixel factor λ determines the theoretical accuracy. Thus, higher measurement accuracy can be achieved with smaller λ. To further accelerate the peak locating process of $r(\boldsymbol{x})$ for a small subpixel factor λ, a three-step matrix-multiply FT approach [22] is employed. Concretely, an initial estimate is obtained with the preliminary subpixel factor $\lambda_1 = 0.5$. Then, the peak is searched around the initial estimate within a 1.5×1.5 pixel region with the subpixel factor $\lambda_2 = \lambda^{1/2}$ as the second step. Finally, the peak location is refined by the full subpixel factor λ, and fine motion $\boldsymbol{m}_f$ with subpixel accuracy is obtained, as illustrated in Fig. 3(b). Thus, the total micromotion can be estimated as $\boldsymbol{m} = \boldsymbol{m}_c + \boldsymbol{m}_f$.

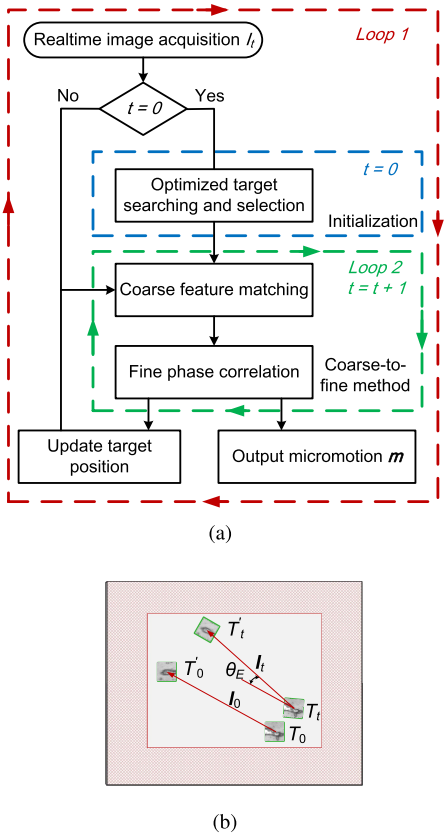

Fig. 4. Diagram of the proposed method. (a) Flowchart of AFMT. (b) Multitarget chosen approach based on the OTS scheme for EAM.

The flowchart of automatic feature-to-phase micromotion tracking (AFMT) is presented in Fig. 4(a), which contains two main loops. The outer loop is for continuous image acquisition, while the OTS scheme is executed as the initial step. The coarse feature matching is then connected to fine phase correlation in the inner loop, where the real-time image sequence can be fed in. The tracking target position is updated in every loop, and the micromotion is measured in the subpixel accuracy. Therefore, the proposed feature-to-phase method balances precision and efficiency by alleviating the high-computational cost from full FOV phase correlation but maintaining high measurement accuracy.

D. Enhanced Angular Measurement (EAM) Method

To meet the needs of tracking extremely small rotation for the three-DOF nanopositioners, an EAM method is proposed based on the multitarget tracking strategy. An extension

approach to the OTS scheme is designed for automatic multiple tracking target selection, as illustrated in Fig. 4(b). Instead of selecting one tracking target in the OTS scheme, the candidate targets are sorted according to their keypoint number. While two candidate targets with the most feature keypoints in the FOV are preferable, the distance D between two candidate targets ought to maintain as large as possible to obtain high angular measurement accuracy. Thus, a length threshold L is set as one of the selection criteria.

After the tracking targets are chosen as T_0 and T_0', both targets are tracked by the AFMT method simultaneously at any time as T_t and T_t'. Since the nanopositioner is considered a rigid body in the FOV of microvision, the measured angle θ_E can be defined as the angle between two vectors $\vec{l}_0 = T_0T_0'$ and $\vec{l}_t = T_tT_t'$. Accordingly,the micro-rotation θ_E as illustrated in Fig. 4(b) is then estimated by

$$\vec{l}_0 \cdot \vec{l}_t = \left\|\vec{l}_0\right\| \left\|\vec{l}_t\right\| \cos\theta_E. \tag{8}$$

Therefore, the measured angle θ_E is obtained, and the marker-free automatic angular measurement is achieved in the microvision-based system for micro-rotation tracking of the nanopositioners. The detailed procedure is presented in Pseudocode 2.

Pseudocode 2: Enhanced Angular Measurement (EAM)

Input : Image sequence I_t.
Output: Micromotion $\boldsymbol{m}$.

procedure Initialization
  if $t == 0$ **then**
    Do OTS scheme and select multipe tracking targets by sorting the candidates according to their keypoint number: $C_1 \geq C_2 \geq C_3 \geq \ldots \geq C_n$;
    for $i \leftarrow 2$ **to** n **do**
      Compute Euclidean distance $D \leftarrow \|C_1 - C_i\|$;
      if $D > L$ **then** `// Maintain D larger than a preset distance L`
        $T_0 \leftarrow C_1, T_0' \leftarrow C_i$;
        Break;
    Construct binary feature descriptors: $b^*(T_0), b^*(T_0')$;
    Compute $\vec{l}_0 = T_0T_0'$;
  return $\vec{l}_0$;
procedure Feature-to-phase angular tracking
  if $t > 0$ **then**
    Extract features from the input image $b^*(I_t)$;
    Compute feature matching: $[\boldsymbol{d}_c, \boldsymbol{d}_c'] \leftarrow min[H(T_{t-1}, I_t), H(T_{t-1}', I_t)]$;
    Locate the ROIs: R_t, R_t';
    Compute phase correlation: $r(T_{t-1}, R_t)$, $r(T_{t-1}', R_t')$;
    Locate the peak: $[\boldsymbol{d}_f, \boldsymbol{d}_f'] \leftarrow argmax[r(T_{t-1}, R_t), r(T_{t-1}', R_t')]$;
    Estimate motion: $[\boldsymbol{d}, \boldsymbol{d}'] \leftarrow [\boldsymbol{d}_c, \boldsymbol{d}_c'] + [\boldsymbol{d}_f, \boldsymbol{d}_f']$;
    Update target location: $[T_t, T_t'] = [T_{t-1}, T_{t-1}'] + [\boldsymbol{d}, \boldsymbol{d}']$;
    Compute $\vec{l}_t = T_tT_t'$;
    Compute θ_E;
  return $\boldsymbol{m} = (\boldsymbol{d}, \theta_E)$;

IV. Simulation Tests of the AFMT Method

A. Validation of the OTS Scheme

Simulation tests were designed to validate the effectiveness and present the advantage of the OTS scheme. For each image, a tracking target was automatically chosen by the OTS scheme, while the other three targets were manually selected by different experts as comparisons. Ten images of the natural surface of the nanopositioner were acquired by the microvision-based system with the FOV of 640 × 480 pixels, and the target size of 100 × 100 pixels were selected. As demonstrated in Fig. 5, the tracking target chosen by the OTS scheme was marked in green, while the other three were manual selection targets. The inconsistent manual targets also indicate the selection variations of human operating personnel. Under the severe Gaussian noise with the variances of $\sigma^2 = 0.001$, the random three-DOF motion was simulated on each image from 0 to 100 pixels and 0° to 10°. If the following feature-to-phase algorithm failed to estimate the simulated motion, or the measurement errors were larger than either 30 pixels or 3°, the target selection would be considered ineffective. Each candidate target was tested 1000 times by the offline simulation. All simulations were programed with Mathworks MATLAB.

Table I lists the results based on different target selections with 40 000 simulations in total. While the OTS scheme achieved a 98.7% effective rate on average with a standard deviation (SD) of 0.8%, the result for the manual target selections was 83.0% with a SD of 12.02%. These results prove the high consistency of the OTS scheme, and demonstrate that different manual target selections will lead to various tracking performances. The results further validate the purpose and advantage of the proposed OTS scheme that can successfully avoid performance deterioration caused by skill variations of the human operators.

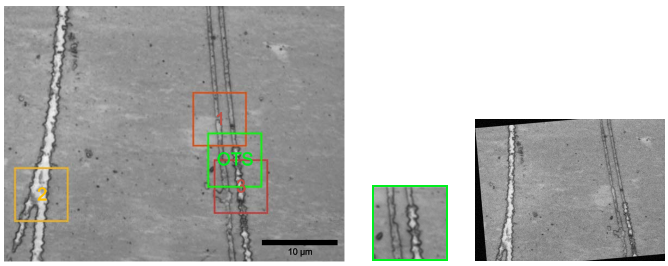

(a) (b) (c)

Fig. 5. Demonstration for evaluating the proposed OTS scheme. (a) Candidate tracking targets by the OTS scheme and human experts. (b) Target automatically selected by the OTS scheme. (c) Image with the simulated three-DOF motion and noises.

B. Robustness Analysis

To validate the robustness of the proposed AFMT method, simulations that consider randomized displacement, rotations, and noise interference were performed. Concretely, displacement (X, Y) in both x- and y-directions from 0 to 100 pixels with the increment of 1 pixel and rotation Θ from 0° to 10°

TABLE I
SIMULATION WITH DIFFERENT TARGET SELECTIONS

No.	1	2	3	4	5	6	7	8	9	10
Expert 1	89.0%	94.9%	84.5%	72.0%	94.2%	99.5%	77.1%	82.0%	92.2%	76.0%
Expert 2	97.3%	89.0%	83.7%	63.3%	70.4%	80.4%	94.8%	63.9%	71.3%	74.9%
Expert 3	98.5%	85.1%	92.9%	97.8%	94.2%	71.3%	73.0%	55.7%	98.1%	74.6%
OTS	99.8%	98.9%	98.2%	99.4%	98.7%	99.6%	98.7%	97.9%	99.0%	97.0%

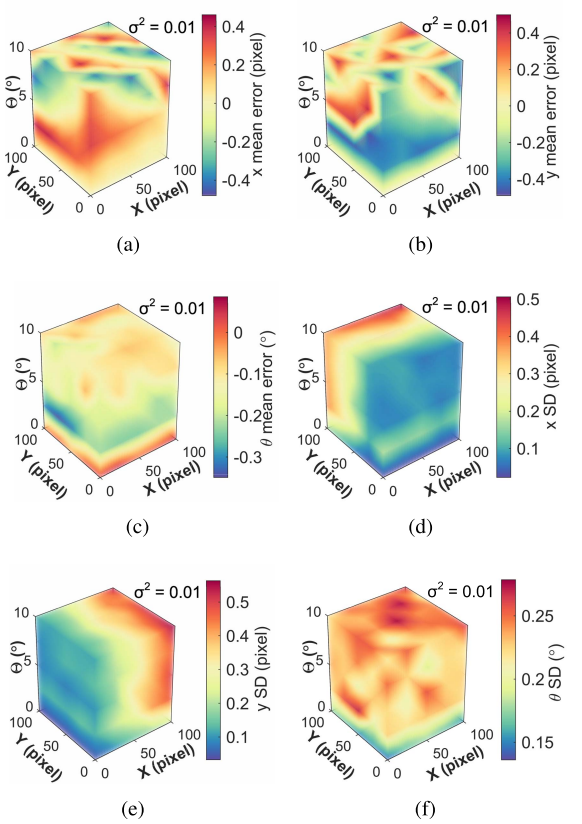

Fig. 6. Visualized mean errors and SDs of each DOF estimation (x, y, θ) with different simulated motion (X, Y, Θ) under noise $(\sigma^2 = 0.01)$. (a)–(c) Estimation errors in x, y, and θ. (d)–(f) SDs in x, y, and θ.

with the increment of 2° were successively applied to simulate the different combinations of three-DOF motion. Meanwhile, severe Gaussian noises with the variances of $\sigma^2 = 0.001$ and $\sigma^2 = 0.01$ were added in all simulations, and the subpixel factor λ was selected as 0.01. For each set of the tests, the simulation was repeated 100 times to verify the robustness of the AFMT method.

The SD of 100 repetitions was calculated to verify the precision, and the average deviation between the simulated motion and the estimated motion by the AFMT method was defined as the mean error. The results are visualized in Fig. 6, where each subfigure corresponds to a set of tests, and the error distribution can be well observed. Concretely, Fig. 6(a)–(c) visualize the estimation errors in x, y, and θ, respectively. These subfigures show that the error distributions are not unified, which demonstrates that the errors were mainly caused by the Gaussian noise $(\sigma^2 = 0.01)$. Fig. 6(d)–(f) visualize the SDs in x, y, and θ, respectively. As can be seen, the larger simulated motion (X, Y, Θ) were input, the higher SDs would occur. This indicates that large motion between two consecutive microvision images is a significant factor in SDs. Table II lists the mean error and the mean SD for each simulation set. Fig. 6 and Table II show that even though the image noise increased from $\sigma^2 = 0.001$ to $\sigma^2 = 0.01$, our proposed method still measured and recorded all the simulated motion with both the mean errors and SDs remaining at the low level. The results indicate that the proposed AFMT method possesses high stability and strong robustness and does not suffer much from performance degradation with increasing noises and motion.

TABLE II
RESULTS WITH THE SIMULATED MOTION (X, Y, Θ)

DOF	Image noise	Mean error	Standard deviation
x (pixel)	$\sigma^2 = 0.001$	0.169	0.112
	$\sigma^2 = 0.01$	0.236	0.229
y (pixel)	$\sigma^2 = 0.001$	0.177	0.123
	$\sigma^2 = 0.01$	0.233	0.235
θ (°)	$\sigma^2 = 0.001$	0.096	0.047
	$\sigma^2 = 0.01$	0.138	0.217

C. Validation of the Real-Time Capability

A series of time cost tests were performed to validate the real-time capability of the proposed AFMT method. Different resolution FOV images were acquired, and different sizes of tracking targets were obtained through the OTS scheme for the tests. The test results are listed in Table III. It can be seen that the time cost increased together with the input image resolution. This is because with higher resolution, more data need to be processed. A smaller tracking target can significantly save the processing time, since the phase correlation in the final step of AFMT method could be time consuming. This also verifies the AFMT method that takes the trade-off between time cost and tracking accuracy. However, if the target size is too small, fewer image features will be contained, and the tracking robustness will be affected.

To determine the size of the tracking target, different sizes of targets were tested by simulation as the same procedure in Section IV-A. The target sizes from 70 × 70 pixels to 140 × 140 pixels were selected for evaluation. The results presented in Fig. 7 show that the tracking effective rate increases till the target size of 100 × 100 pixels, in which the AFMT method can achieve a balanced tracking performance between accuracy and efficiency with around 100 Hz. Moreover, the simulation was programed by MATLAB. If an additional conversion to a more efficient programming language such as C++ was conducted, the time cost would be expected to be further reduced. Therefore, in terms of our previous

TABLE III
EFFICIENCY OF THE AFMT METHOD

No.	Target size (pixel)	Time cost with different resolution (ms)		
		640 × 480	800 × 600	1024 × 768
1	100	9.92	11.65	15.22
2	150	12.97	14.51	18.34
3	200	16.46	17.97	21.20

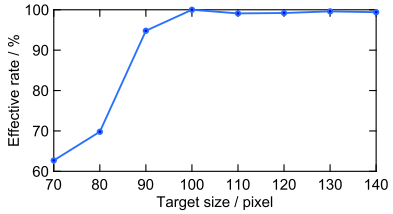

Fig. 7. Effective rate of tracking targets with different sizes.

research [23], the proposed AFMT method would be fast enough for the tracking control of the robotic nanopositioners.

D. Comparisons of the AFMT Method With Other Tracking Algorithms

Comparisons with other state-of-the-art approaches from different categories of existing microvision-based methods in precision motion measurement were conducted in this section to highlight the advantages of the proposed AFMT method. Concretely, the improved SSD template matching methods with the exhaustive searching-based approach (ES) and iterative searching-based approach (IS) [24], the feature matching method (ORB) [25], and the enhanced phase correlation (EPC) method [22] were employed. The parameters of the aforementioned methods were properly chosen to maximize their performances, where the iteration was set to 15 for IS and the subpixel factor λ was set to 0.01 for EPC. The size of the microscope image and the tracking target was 640 × 480 pixels and 100 × 100 pixels, respectively. The input motion with the increment of 0.1 pixel from the range of 0–10 pixel was simulated under the noise $\sigma^2 = 0.001$, and all the methods were implemented to track this motion.

Each method took 100 measurements, while the tracking errors and the computational costs were calculated and recorded. Boxplot representation is used to illustrate the tracking error distribution, as shown in Fig. 8(a), and the average time costs of each method are presented in Fig. 8(b). As summarized in Table IV, for template matching approaches, compared to the ES method with an average time cost of 80.94 ms, IS method can decrease the computational cost to 16.19 ms. However, a significantly larger tracking error (8.48 pixel) is observed for IS method. This is because IS method searches and locates the target near the previous template for high efficiency, thereby IS method is only capable of small motion measurement between two consecutive frames and would cause large tracking errors when the motion is beyond the iteration range. EPC method shows the highest tracking accuracy (0.13 pixel), though its computational cost (92.91 ms) is the most expensive due to the properties of phase correlation. On the other hand, ORB method processes the best

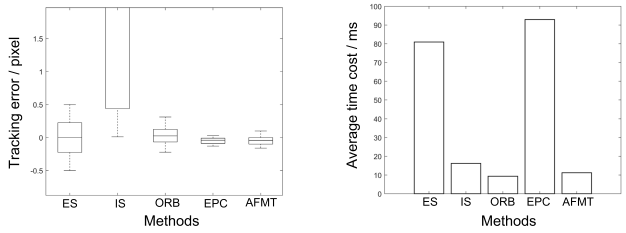

(a) (b)

Fig. 8. Comparison of the AFMT method with other state-of-the-art microvision-based tracking methods by (a) tracking accuracy and (b) efficiency. The height of the box in the boxplot representation denotes the main distribution of the tracking errors, the line inside the box represents the medium value of the errors, and the dash lines outside the box are the maximum and minimum values.

TABLE IV
SIMULATION OF DIFFERENT MICROVISION-BASED METHODS

Methods	ES	IS	ORB	EPC	AFMT
Maximum error (pixel)	0.50	8.48	0.31	0.13	0.19
Mean error (pixel)	0.24	3.46	0.11	0.05	0.04
Standard deviation (pixel)	0.29	2.91	0.09	0.04	0.05
Average time cost (ms)	80.94	16.19	8.96	92.91	10.22

efficiency (8.96 ms) due to the fast sparse point corresponding. Nevertheless, the proposed AFMT method enjoys a higher tracking accuracy (0.11 pixel) than ORB method (0.31 pixel). At the same time, the time cost of the proposed method just slightly increases by 1.26 ms and is much smaller than EPC method. Besides, the SDs for ES, IS, ORB, EPC, and AFMT methods are 0.24, 3.46, 0.11, 0.05, and 0.04 pixels, respectively, which further confirms the stable tracking performance of the proposed AFMT method. The results indicate that the AFMT method has achieved an ideal balance between accuracy and efficiency using the feature-to-phase strategy and has shown an excellent performance in general compared to other tracking algorithms for microvision-based measurement systems.

V. ONLINE EXPERIMENTS OF THE MICROVISION-BASED MEASUREMENT SYSTEM

A. Accuracy and Precision Evaluation

Online experiments have been conducted in different experimental settings to demonstrate various performances of the proposed microvision-based measurement system. A three-DOF robotic compliant nanopositioner was manufactured in our previous work [26] and used in the experiments. Driven by the piezoelectric actuators (PAs) (PI Ceramic GmbH P-841.2B, Germany), the nanopositioner can provide three-DOF micromotion within the range 30 μm × 30 μm × 4.2 mrad under control from the single-board controller (dSPACE DS1104, Germany) inserted in the IPC.

CSs (0.002% dynamic resolution, 1024 Hz bandwidth, PI Ceramic GmbH D-E 20.200, Germany) were also employed to compare with the proposed microvision-based measurement system. Since CS is a one-DOF professional instrument, trigonometry has to be applied to the outputs of six CSs for calculating three-DOF measurement, as exhibited in Fig. 9(a). The microvision-based measurement system was

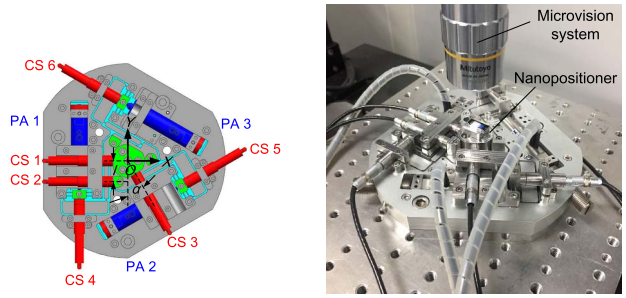

Fig. 9. Experimental setup for accuracy, precision, and resolution evaluation. (a) Diagram of the design and coordinate of the nanopositioner. (b) Nanopositioner in the online experiments.

calibrated by the calibration process in [27], and a total magnification of 16.25 was obtained. The target size of 100 × 100 and the image resolution of 640 × 480 were selected, which corresponded to 216.62 × 162.46 μm FOV. With the CS measurements as the reference, the accuracy of the microvision-based method was testified by simultaneously tracking the micromotion of the robotic nanopositioner, as presented in Fig. 9(b). A box-shape trajectory within the workspace of the nanopositioner was designed for both static and dynamic measurement, as illustrated in Fig. 10(a), which contains 25 stopping points. Whenever the nanopositioner reached a stopping point, it would stay for a stop time t_s = 2 s, then traveled to the next stopping point in a moving time t_m = 1 s, while the nanopositioner angle kept at 0.

The tracking results are visualized in Fig. 10(b), which shows the measurements from the microvision are highly in line with the CS measurements. Since the tracking frequency of CS is much larger than the microvision-based measurement system, the dynamic tracking error can be defined as

$$e_d = \max_{1 \le t \le k} |\boldsymbol{m}_t - \boldsymbol{m}_{\mathrm{CS}}| \tag{9}$$

where k is the frame number of microvision-based system, $\boldsymbol{m}_t$ is the measurement result of microvision, $\boldsymbol{m}_{\mathrm{CS}}$ is the closest CS data at time t. The maximum dynamic tracking error e_d of the entire trajectory was obtained as 93 nm. The measurement results corresponding to each stopping point were extracted to evaluate the static measurement accuracy. In x- and y-directions, the maximum static measurement error e_s of ±31 and ±40 nm were, respectively, obtained, as shown in Fig. 10(c). The input displacement loss was also observed, which verifies the hysteresis effect and compliant deformation of the piezo-actuated compliant mechanisms [7]. Fig. 10(d) shows the angular measurement results that distributed around ± 0.02 rad. This is reasonable as environmental disturbances and image noises caused intensity variation during the tracking process, while the intensity centroid approach in the feature-based method was sensitive to intensity fluctuation. As a result, the EAM method is needed for micro-rotation tracking, as presented in Section V-B.

To evaluate the precision of the proposed microvision-based measurement system, the SD was separately calculated at each stopping point, where the nanopositioner was measured. On average, the SDs of the proposed method were 14 nm in the x-direction and 8 nm in the y-direction, respectively,

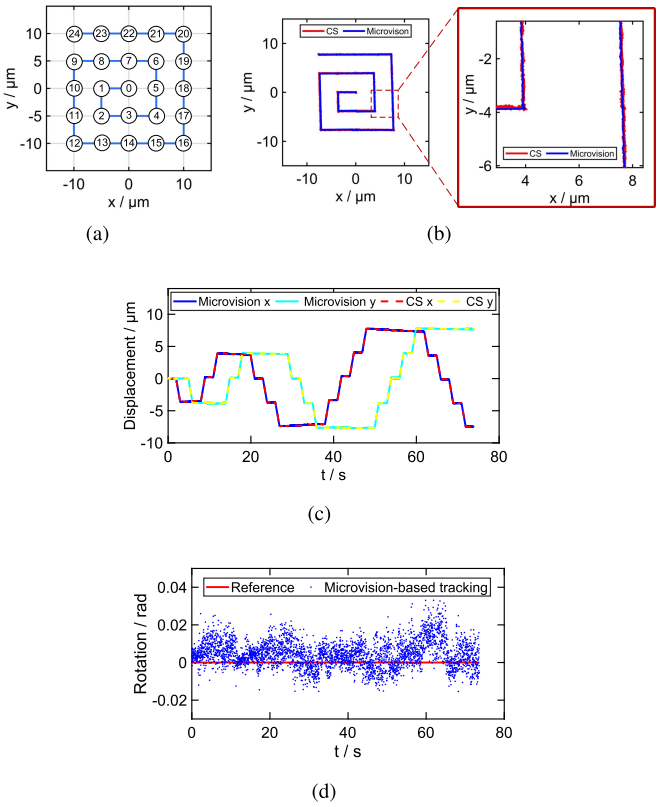

Fig. 10. Tracking accuracy evaluation. (a) Planned trajectory of the nanopositioner. (b) Tracking results from the microvision system and CS with a zoom-in subfigure. (c) Detailed tracking results in each direction. (d) Angular tracking results.

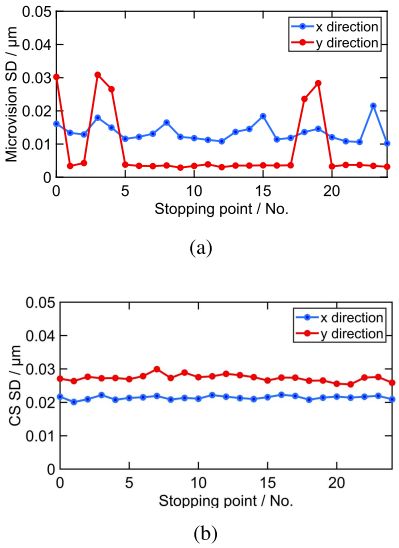

Fig. 11. Tracking precision evaluation. (a) Experimental results of the proposed method. (b) Experimental results of CS method.

which were slightly smaller than 21 and 27 nm by the CS measurement, as shown in Fig. 11. Therefore, the displacement measurement accuracy and precision are high within the FOV of the proposed microvision-based measurement system.

B. Enhanced Angular Tracking for Micro-Rotation

To validate the proposed EAM method, the experiment of micro-rotation was performed. With the same experimental

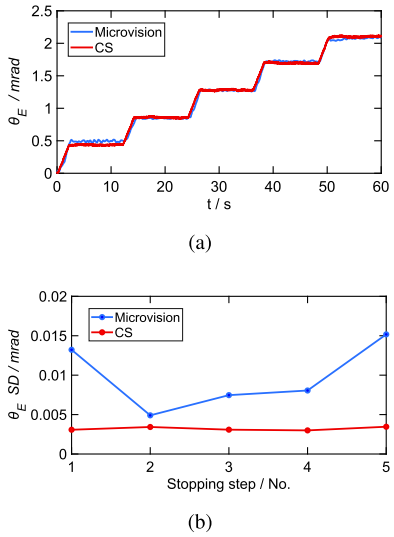

Fig. 12. Angular measurement based on the EAM method. (a) Experimental results of angular tracking accuracy. (b) SDs from the microvision system and CS.

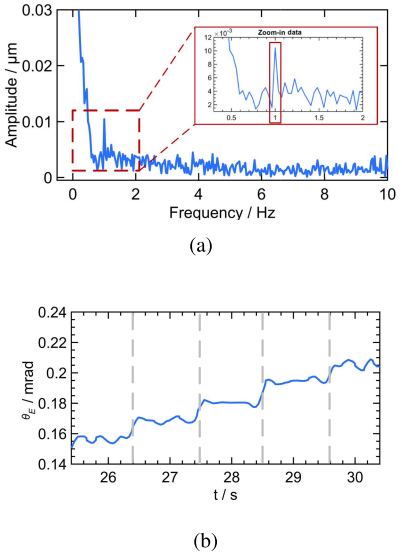

Fig. 13. Experimental results of the resolution tests for the microvision-based system. (a) Position tracking resolution. (b) Angular tracking resolution.

setup in Section V-A, the nanopositioner was rotated step by step between 0 and 2.5 mrad. A micro-rotation of 0.5 mrad for each step was input, and the moving time t_s of each step was 2 s, and the stopping time t_s was 10 s. The CSs were also employed as comparisons. As presented in Fig. 12(a), the tracking results from the microvision system coincided with the CSs. The dynamic angular tracking errors e_d were calculated, where the maximum tracking error of 96 μrad was recorded. The SDs at each stopping step were also calculated and plotted in 12(b). The average SDs from the microvision system and CS were 8.5 and 3.1 μrad, respectively, where both show very high precision.

The experimental results indicate that the EAM method can significantly improve the angular measurement performance of the microvision-based system for micro-rotation. This method takes advantage of the high accuracy of position localization from AFMT, and thereby is able to complete with the CS in angular measurement.

C. Resolution Tests

The tracking resolution is defined as the smallest change that can be detected. It is desirable to detect the motion as fine as possible, even though it is merged in the noise of a larger magnitude. To detect the smallest displacement despite noises, the resolution tests were performed using the frequency domain analysis approach [28]. A pulse sequence of period 1 s with an amplitude of 10 nm was input to the nanopositioner, and the motion was tracked using the proposed method. The FT was applied to the microvision data, and if the peak of the resulting curve is found at the expected frequency, the displacement would be detected, so the microvision-based method has a resolution at least equal to its amplitude. The experimental results were plotted in Fig. 13(a), where a spectral lobe was observed at 1 Hz with an amplitude around 10 nm, which corresponded to the input signal. This demonstrates the position tracking resolution of the proposed microvision-based measurement system is higher than 10 nm.

The angular measurement resolution tests were also conducted, while a signal with a frequency of 1 Hz and an amplitude of 10 μrad was input for micro-rotation. As presented in Fig. 13(b), visible angular changes can be observed at each signal period, which indicates at least 10 μrad angular tracking resolution is achieved using the EAM method.

D. Velocity Estimation

In addition to position and angular tracking, it is also preferable to achieve velocity sensing of robotic nanopositioners based on microvision. Therefore, we explore the velocity estimation based on the proposed measurement system. Since velocity is defined as the rate of change of displacement, by acquiring the time stamp of each frame from the inner cock of the CMOS sensor, velocity can be calculated as the detected displacement $\boldsymbol{d}_t$ divided by the time interval Δt between two consecutive frames

$$\boldsymbol{v}_t = \frac{\boldsymbol{d}_t}{\Delta t}. \tag{10}$$

The supplementary experiments were carried out on the setup in Fig. 14(a). A circular trajectory with a radium of 12 μm and a moving time of 4 s was planned to demonstrate the velocity estimation of the nanopositioner. The fourth-order low-pass Butterworth filter [29] was used to filter out noise interference. The trajectory tracking result and its corresponding velocity estimation from the microvision system are shown in Fig. 14(b) and (c), respectively, where the smooth velocity curves in both x- and y-directions verify the effectiveness of velocity estimation.

To quantitatively investigate the velocity estimation accuracy, a laser vibrometer (LV) (2000 Hz frequency, 0.01 μm/s resolution, Polytec OFV-5000, Germany) was employed. Since the LV is only capable of measuring one-DOF velocity, specifically a one-DOF trajectory alone the y-direction was designed for the experiment, as shown in Fig. 14(d). Both the microvision system and the LV simultaneously estimated the

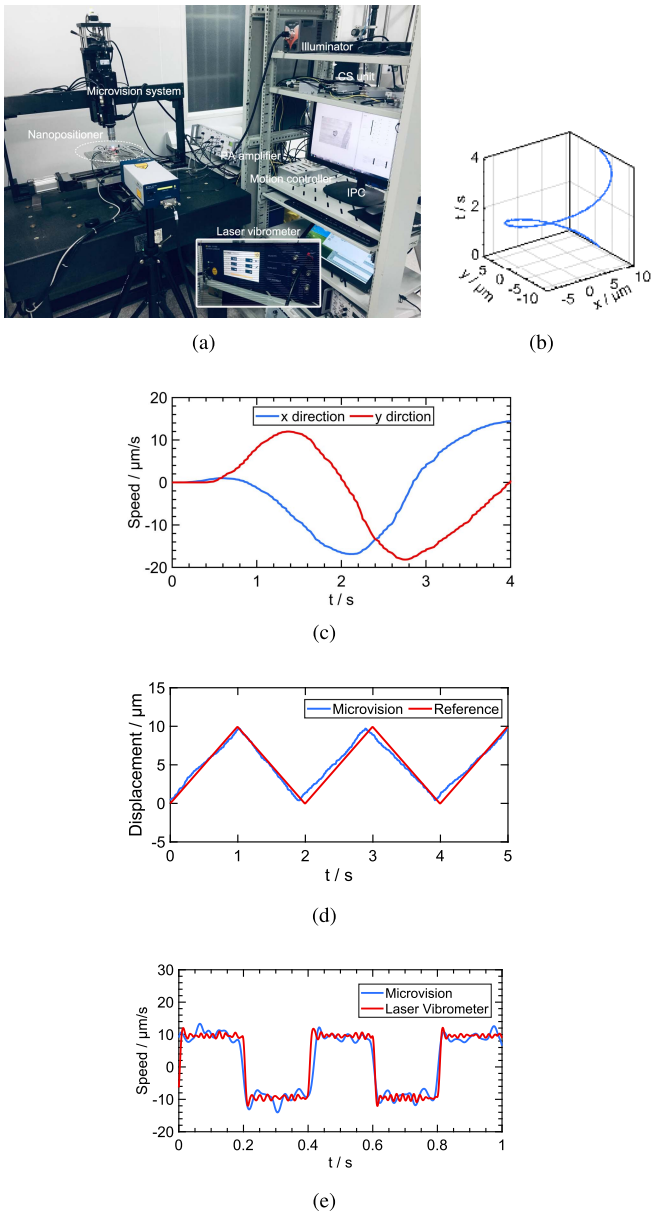

Fig. 14. Experiments for velocity estimation. (a) Experimental setup. (b) Tracking results in the $x - y - t$ space. (c) Corresponding estimated velocity in each direction. (d) Linear trajectory planning and tracking results for velocity validation. (e) Velocity estimation compared with the LV.

velocity of the nanopositioner, and the experimental results are shown in Fig. 14(e). The maximum deviation is observed as 3 μm/s, and there are two main reasons that may lead to this deviation: 1) LV was set up on the ground instead of the vibration table of the microvision-based system due to the experimental limitation, hence, two measuring systems suffered from different environmental vibrations and 2) the measurement frequencies of the two methods were also different in the experiment, thus, the measurement time-axes cannot be precisely matched for calculating the dynamic error of velocity estimation. Nevertheless, the results from the proposed microvision-based measurement system still coincide with the LV's. The velocity estimation also enjoys multi-DOF ability with almost no additional cost. Therefore, it is a beneficial extension and complement to the microvision-based system.

VI. Conclusion

A microvision-based measurement system for precision motion sensing of the robotic nanopositioners has been developed in this study. The marker-free AFMT was designed, which consists of the OTS scheme and the feature-to-phase tracking method. The EAM method for micro-rotation tracking and velocity estimation method were also proposed, which enrich the functions of the microvision-based measurement system. Simulations were performed to validate the AFMT method in terms of target selection, robustness, and efficiency compared to other microvision-based methods. Online experiments were conducted for three-DOF motion tracking of the robotic nanopositioner to verify the accuracy, precision, and resolution of the microvision-based measurement system with comparisons to professional instruments, i.e., CS and VM. With the better extensibility and flexibility, the proposed microvision-based motion measurement system not only can be a competitive alternative to traditional instruments in micro/nanomanipulation for motion measurement of micro/nanopositioning stages, but also has the potential to track manipulated micro-objects with a certain extent of deformation, and end-effectors, such as the microgripper, micropipette, and cantilever.

Acknowledgment

The authors gratefully acknowledge the support agency.

References

[1] P. Wang and Q. Xu, "Design and testing of a flexure-based constant-force stage for biological cell micromanipulation," *IEEE Trans. Autom. Sci. Eng.*, vol. 15, no. 3, pp. 1114–1126, Jul. 2017.

[2] T. Tuma, A. Sebastian, J. Lygeros, and A. Pantazi, "The four pillars of nanopositioning for scanning probe microscopy: The position sensor, the scanning device, the feedback controller, and the reference trajectory," *IEEE Control Syst.*, vol. 33, no. 6, pp. 68–85, Dec. 2013.

[3] Y. L. Zhang, M. L. Han, M. Y. Yu, C. Y. Shee, and W. T. Ang, "Automatic hysteresis modeling of piezoelectric micromanipulator in vision-guided micromanipulation systems," *IEEE/ASME Trans. Mechatronics*, vol. 17, no. 3, pp. 547–553, Jun. 2012.

[4] H. Xie et al., "High-speed AFM imaging of nanopositioning stages using H_∞ and iterative learning control," *IEEE Trans. Ind. Electron.*, vol. 67, no. 3, pp. 2430–2439, Mar. 2020.

[5] M. Torralba, J. Yagüe-Fabra, J. Albajez, and J. Aguilar, "Design optimization for the measurement accuracy improvement of a large range nanopositioning stage," *Sensors*, vol. 16, no. 1, p. 84, Jan. 2016.

[6] X. Li, W. Gao, H. Muto, Y. Shimizu, S. Ito, and S. Dian, "A six-degree-of-freedom surface encoder for precision positioning of a planar motion stage," *Precis. Eng.*, vol. 37, no. 3, pp. 771–781, 2013.

[7] R. Wang and X. Zhang, "Optimal design of a planar parallel 3-DOF nanopositioner with multi-objective," *Mech. Mach. Theory*, vol. 112, pp. 61–83, Jun. 2017.

[8] S. Yao, H. Li, S. Pang, B. Zhu, X. Zhang, and S. Fatikow, "A review of computer microvision-based precision motion measurement: Principles, characteristics, and applications," *IEEE Trans. Instrum. Meas.*, vol. 70, pp. 1–28, 2021.

[9] C. Zhao, C. Cheung, and M. Liu, "Integrated polar microstructure and template-matching method for optical position measurement," *Opt. Exp.*, vol. 26, no. 4, pp. 4330–4345, 2018.

[10] H. Li, B. Zhu, Z. Chen, and X. Zhang, "Realtime in-plane displacements tracking of the precision positioning stage based on computer microvision," *Mech. Syst. Signal Process.*, vol. 124, pp. 111–123, Jun. 2019.

[11] D. G. Lowe, "Distinctive image features from scale-invariant keypoints," *Int. J. Comput. Vis.*, vol. 60, no. 2, pp. 91–110, 2004.
[12] B. S. Reddy and B. N. Chatterji, "An FFT-based technique for translation, rotation, and scale-invariant image registration," *IEEE Trans. Image Process.*, vol. 5, no. 8, pp. 1266–1271, Aug. 1996.
[13] A. N. Andre, P. Sandoz, B. Mauze, M. Jacquot, and G. J. Laurent, "Sensing one nanometer over ten centimeters: A microencoded target for visual in-plane position measurement," *IEEE/ASME Trans. Mechatronics*, vol. 25, no. 3, pp. 1193–1201, Jun. 2020.
[14] C. Yamahata, E. Sarajlic, G. J. M. Krijnen, and M. A. M. Gijs, "Subnanometer translation of microelectromechanical systems measured by discrete Fourier analysis of CCD images," *J. Microelectromech. Syst.*, vol. 19, no. 5, pp. 1273–1275, Oct. 2010.
[15] S. Yao, H. Li, S. Pang, L. Yu, S. Fatikow, and X. Zhang, "Motion measurement system of compliant mechanisms using computer microvision," *Opt. Exp.*, vol. 29, no. 4, pp. 5006–5017, 2021.
[16] E. Rosten, R. Porter, and T. Drummond, "Faster and better: A machine learning approach to corner detection," *IEEE Trans. Pattern Anal. Mach. Intell.*, vol. 32, no. 1, pp. 105–119, Jan. 2010.
[17] H. Bay, A. Ess, T. Tuytelaars, and L. Van Gool, "Speeded-up robust features (SURF)," *Comput. Vis. Image Understand.*, vol. 110, no. 3, pp. 346–359, 2008.
[18] W. Huang, L.-D. Wu, H.-C. Song, and Y.-M. Wei, "RBRIEF: A robust descriptor based on random binary comparisons," *IET Comput. Vis.*, vol. 7, no. 1, pp. 29–35, Feb. 2013.
[19] M. Muja and D. G. Lowe, "Fast approximate nearest neighbors with automatic algorithm configuration," *VISAPP*, vol. 2, nos. 331–340, p. 2, 2009.
[20] S. Walfish, "A review of statistical outlier methods," *Pharmaceutical Technol.*, vol. 30, no. 11, p. 82, 2006.
[21] H. Foroosh, J. B. Zerubia, and M. Berthod, "Extension of phase correlation to subpixel registration," *IEEE Trans. Image Process.*, vol. 11, no. 3, pp. 188–200, Mar. 2002.
[22] M. Guizar-Sicairos, S. T. Thurman, and J. R. Fienup, "Efficient subpixel image registration algorithms," *Opt. Lett.*, vol. 33, no. 2, pp. 156–158, 2008.
[23] J. Gan, X. Zhang, H. Li, and H. Wu, "Full closed-loop controls of micro/nano positioning system with nonlinear hysteresis using microvision system," *Sens. Actuators A, Phys.*, vol. 257, pp. 125–133, Apr. 2017.
[24] H. Li, X. Zhang, B. Zhu, and S. Fatikow, "Online precise motion measurement of 3-DOF nanopositioners based on image correlation," *IEEE Trans. Instrum. Meas.*, vol. 68, no. 3, pp. 782–790, Mar. 2019.
[25] E. Rublee, V. Rabaud, K. Konolige, and G. Bradski, "ORB: An efficient alternative to SIFT or SURF," in *Proc. Int. Conf. Comput. Vis.*, Nov. 2011, pp. 2564–2571.
[26] R. Wang and X. Zhang, "Parameters optimization and experiment of a planar parallel 3-DOF nanopositioning system," *IEEE Trans. Ind. Electron.*, vol. 65, no. 3, pp. 2388–2397, Mar. 2018.
[27] H. Li, X. Zhang, H. Wu, and J. Gan, "Line-based calibration of a micro-vision motion measurement system," *Optics Lasers Eng.*, vol. 93, pp. 40–46, Jun. 2017.
[28] V. Guelpa, P. Sandoz, M. A. Vergara, C. Clévy, N. L. Fort-Piat, and G. J. Laurent, "2D visual micro-position measurement based on intertwined twin-scale patterns," *Sens. Actuators A, Phys.*, vol. 248, pp. 272–280, Sep. 2016.
[29] I. W. Selesnick and C. S. Burrus, "Generalized digital Butterworth filter design," *IEEE Trans. Signal Process.*, vol. 46, no. 6, pp. 1688–1694, Jun. 1998.

Sheng Yao received the B.E. degree in mechatronics engineering and the Ph.D. degree in mechanical engineering from the South China University of Technology, Guangzhou, China, in 2016 and 2021, respectively.

He was a joint Ph.D. Student at the Department of Mechanical and Industrial Engineering, University of Toronto, Toronto, ON, Canada, from 2018 to 2019. He is currently a Lecturer with the School of Biomedical Engineering, Southern Medical University, Guangzhou. His research interests include high-precision vision systems and vision-based control for micromanipulation, with applications to microelectromechanical systems (MEMS) and cell surgery.

Xianmin Zhang received the Ph.D. degree from the Beijing University of Aeronautics and Astronautics, Beijing, China, in 1993.

Since 2010, he has been the Director of the Guangdong Key Laboratory of Precision Equipment and Manufacturing Technology, South China University of Technology, Guangzhou, China. Since 2013, he has been the Dean and the Chair Professor of the School of Mechanical and Automotive Engineering, South China University of Technology. His research interests include robotics, precision instrument analysis and design, dynamics, and vibration control of mechanisms.

Benliang Zhu received the Ph.D. degree in mechanical engineering from the South China University of Technology, Guangzhou, China, in 2014.

He is currently a Professor with the South China University of Technology. His current research interests include microelectromechanical systems (MEMS) technique, precision positioning, and manipulation in the microscale and nanoscale.

Hai Li received the Ph.D. degree in mechanical engineering from the South China University of Technology, Guangzhou, China, in 2018.

He spent one year as a Post-Doctoral Fellow at the Division for Microrobotics and Control Engineering (AMiR), University of Oldenburg, Oldenburg, Germany. He is currently an Associate Professor with the South China University of Technology. His research interests include vision-based precision measurement and servo control, and micro-/nano positioning and manipulation.

Longhuan Yu received the M.S. degree in mechanical engineering from the South China University of Technology, Guangzhou, China, in 2019, where he is currently pursuing the Ph.D. degree in mechanical engineering.

His current research interests include nanopositioning and vibration control.

Sergej Fatikow received the Ph.D. degree in electrical engineering and computer science from Ufa State Aviation Technical University, Ufa, Russia, in 1988.

In 1990, he moved to the University of Karlsruhe, Karlsruhe, Germany, where he initiated the new research field of microrobotics. Since 2001, he has been a Full Professor with the Department of Computing Science and the Head of the Division for Microrobotics and Control Engineering (AMiR), University of Oldenburg, Oldenburg, Germany. His research interests include micro and nanorobotics automation at nanoscale, sensor feedback at nanoscale, and neurofuzzy robot control.